Enhanced Self-Seeding with Ultrashort Electron Beams

Erik Hemsing,* Aliaksei Halavanau,† and Zhen Zhang‡
SLAC National Accelerator Laboratory, Menlo Park, California 94025, USA

(Received 7 February 2020; revised 15 June 2020; accepted 1 July 2020; published 22 July 2020)

We describe a new method to produce intensity stable, highly coherent, narrow-band x-ray pulses in self-seeded free electron (FEL) lasers. The approach uses an ultrashort electron beam to generate a single spike FEL pulse with a wide coherent bandwidth. The self-seeding monochromator then notches out a narrow spectral region of this pulse to be amplified by a long portion of electron beam to full saturation. In contrast to typical self-seeding where monochromatization of noisy self-amplified spontaneous emission pulses leads to either large intensity fluctuations or multiple frequencies, we show that this method produces a stable, coherent FEL output pulse with statistical properties similar to a fully coherent optical laser.

DOI: 10.1103/PhysRevLett.125.044801

Self-seeded x-ray free electron lasers (FELs) use relativistic electron beams to produce intense, narrow-band x-ray pulses for a wide array of high resolution science applications. They work by effectively splitting a single pass, high-gain FEL into two sections. In the first section (i.e., the SASE FEL), the electron beam produces x rays by self-amplified spontaneous emission (SASE). Originating from shot noise, the SASE pulse is stochastic in nature and has the features of chaotic polarized radiation [1]. As such, it contains many uncorrelated temporal and frequency spikes. The SASE spectrum is then frequency filtered with a monochromator (diffraction grating or crystal), which isolates a narrow region of SASE frequencies for amplification [2,3]. In the second section (the seeded FEL), the filtered light (i.e., the seed) is placed back on the electron beam and amplified to saturation. This technique has been used to increase the coherence of x-ray FELs and to produce pulses with relative bandwidths $\sim 10^{-4}$ at both hard and soft x-ray wavelengths [4,5].

Generally, the first-stage SASE pulse is produced in the linear regime by an electron beam (e-beam) that is much longer than the FEL cooperation time, $\tau_c = 1/2\sqrt{3}\rho\omega_0$, where ω_0 is the radiation frequency and ρ is the FEL parameter [6]. The cooperation time is the slippage accrued over an exponential gain length and sets the approximate temporal scale over which the amplified radiation is coherent. Long flat e-beams with duration $T \gg 2\pi\tau_c$ contain a large number of coherent temporal spikes. Accordingly, the SASE spectrum, which spans a bandwidth $\sigma_A \approx \rho\omega_0 = 1/2\sqrt{3}\tau_c$, contains a large number of frequency spikes, each with average width $\Delta\omega_c = 2\pi/T$. The average number of spikes that then pass through the self-seeding filter depends on the monochromator (mono) linewidth σ_m. If $\sigma_m \ll \Delta\omega_c$ then, on average, the seed consists of a single coherent spike, but exhibits large intensity fluctuations. If the filter bandwidth is much larger than a single frequency spike, then the seed contains multiple spikes, but the integrated fluctuations are reduced. Thus, with SASE from traditional long beams there is a fundamental trade-off between number of spikes (coherence) and fluctuations (stability). For the soft x-ray (SXR) self-seeding system at Linac Coherent Light Source (LCLS) [4], the effective mono bandwidth ($\sigma_m \approx 85$ meV rms at 1 keV photon energies) passes $M = 4$–5 coherent modes with the nominal $T \geq 50$ fs e-beam, and exhibits the associated $\sigma_\mathcal{E} = 1/\sqrt{M}$ level of relative pulse energy fluctuations during exponential growth in the seeded stage [7]. While saturation effects can eventually reduce the fluctuations in the amplified seed, it lacks full temporal coherence. Further, this precludes maximal energy extraction with strong downstream undulator tapering [8], and the buildup of SASE in the regions between coherent spikes generates an undesirable spectral pedestal [4,9].

Here we propose a simple new self-seeding scheme that reduces the level of fluctuations to the few percent level while also maintaining a temporally coherent FEL output. In this arrangement the FEL statistically behaves less like a chaotic source and more like an ideal laser [10] or an externally seeded FEL [11]. Inspired by the proposal to produce single spike FEL pulses in Ref. [12] and recent work on the generation of stable sub-fs pulses at LCLS [13,14], this scheme uses an ultrashort, high current portion of electron beam with duration

$$T \approx 2\pi\tau_c = \pi/\sqrt{3}\rho\omega_0 \tag{1}$$

to produce a saturated, single spike ($M \approx 1$) SASE x-ray FEL pulse incident on the self-seeding mono. The mono then selects a narrow section of the coherent spectrum to act as a seed, essentially acting as a pulse stretcher of the saturated single spike SASE pulse. The concept is illustrated in Fig. 1. The self-seeding chicane delay is adjusted to place the seed on a different, longer portion of e-beam with lower current that amplifies the narrow-band seed to

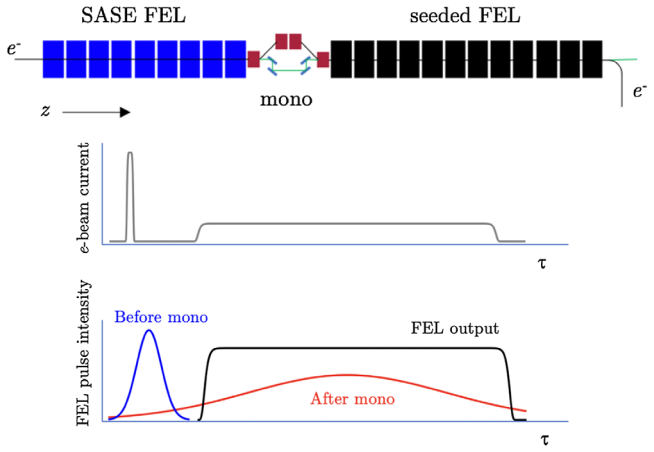

FIG. 1. Illustration of the proposed scheme. Top: Layout of the SXR self-seeding beam line (not to scale). Below: A high-current, short pulse portion of e-beam lases to saturation in the SASE section to produce a single spike pulse (blue). After the narrow-band monochromator (mono), the spike is stretched (red) to overlap a longer flat-current section of e-beam, and then amplified to saturation, producing a stable single mode long pulse in the FEL output (black). The long portion of the beam does not lase strongly in the SASE section due to low current and/or strong undulator tapering, but does lase strongly in the seeded section.

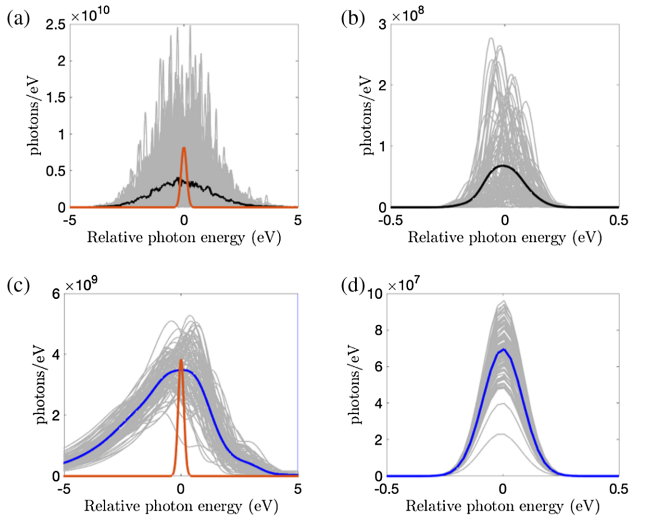

FIG. 2. Comparison of spectra when seeding with a long SASE pulse (black) versus a saturated short SASE pulse (blue) at 1 keV photon energy modeled with 100 GINGER simulations. With a long e-beam $T \gg 2\pi\tau_c$ the incident SASE frequencies on the mono filter (red) fluctuate stochastically, resulting in a fluctuating seed (b). With a short e-beam $T = 2\pi\tau_c$ (c), the incident single spike spectrum is much more stable, as is the single-mode seed (d).

saturation. This scheme requires no additional x-ray optics, only tailoring of the incoming e-beam in a manner similar to previous efforts to produce sub-fs pulses [14–16], double-bunch configurations [17,18], or by shaping in the laser heater (see Supplemental Material [19]).

In this technique it is important that lasing of the long portion of the e-beam in the SASE section is weak so that it remains unspoiled for seeding. This may be accomplished simply by sufficiently low current (see Supplemental Material [19]), or by active suppression, e.g., in the laser heater [20], with the fresh-slice technique [21], or even with a strong undulator taper [22]. Likewise, it is desirable to prevent further FEL emission in the seeded stage by the spent high current spike. In start-to-end simulations (see Supplemental Material [19]), we find that the beam is sufficiently spoiled by saturation in the first stage that it contributes only negligibly in the seeded stage. Otherwise, in some self-seeding designs, dispersion in the chicane, used to compensate the optical delay, can decompress the current spike by exploiting the large energy spread.

The distinction between this approach and typical self-seeding is illustrated in Fig. 2. We find that this technique, which is a version of fresh bunch self-seeding [23], has several advantages. First, the short e-beam produces a single spectral spike pulse that fully covers the seeded FEL bandwidth, so there is always a single spectral mode with significant power within the mono bandwidth. Second, the high current spike reaches saturation at the mono, which significantly reduces intensity fluctuations of the seed compared to normal self-seeding where the signal is filtered early in the linear regime. Third, because the short pulse saturates, the peak seed power can be orders of magnitude higher at the start of the seeded section than in normal self-seeding, but with only modest pulse energy. The higher power seed helps stabilize the final FEL output by vastly exceeding the shot noise power (here by 10^3), while the x-ray energy deposition on the self-seeding optics is kept small to prevent damage. Fourth, seeding with a high power, stable single mode then enables reliable downstream amplification and strong tapering to maximize FEL output within the narrow seeded bandwidth, and with minimal spectral SASE pedestal. Finally, this scheme enables some unique coherent tailoring of the FEL seed. For example, with soft x rays, different grating surface designs would allow near-transform limited tuning of the FEL output by varying σ_m without changing the number of seed modes, or even seeding multiple phase-stable colors as we will show.

This concept builds on the statistical properties of ultrashort SASE FEL pulses near saturation, which have been studied previously. In Ref. [24], numerical studies indicated that relative pulse energy fluctuations in the saturation (nonlinear) regime are reduced to the $\sigma_\mathcal{E} = 10\%$–$20\%$ level when T shrinks to become comparable with $2\pi\tau_c$. These results are in agreement with experimental measurements [25], and are attributed to the strong slippage effects. In the linear regime, slippage smooths the initial shot noise, but there are still fluctuations in the onset of lasing. Eventually, however, the power and e-beam

TABLE I. LCLS-II SXR beam line parameters

Parameter	Value	Units
Beam energy, E	4	GeV
Undulator strength (rms) K	2.295 71	⋯
Undulator period, λ_u	3.9	cm
Undulator section length, L_u	3.4	m
Undulator drift length, L_{ud}	1.0	m
Fundamental energy, $\hbar\omega_0$	620	eV
Monochromator bandwidth (rms), σ_m	85	meV

bunching saturate and the coherent pulse slips out front of the e-beam, significantly stabilizing the output. We find that, after spectral filtering through the narrow-band mono, these pulses serve as stable and coherent seeds for subsequent amplification.

To illustrate, we consider the case of the LCLS-II SXR beam line at SLAC (see Table I) with an ideal beam. We modeled the system in the conventional FEL codes GENESIS [26] and GINGER [27], with both showing nearly identical results. Lasing is simulated at a $\hbar\omega_0 = 620$ eV fundamental photon energy ($\lambda = 2$ nm) in both the SASE and seeded sections. First, the short pulse SASE section is simulated over multiple runs to generate a statistical dataset for analysis. The output fields are then monochromatized using a 2% efficiency, $\sigma_m = 85$ meV rms width Gaussian filter (identical to the LCLS design) positioned at the average spectral peak to extract the seed fields. These 3D fields are then used as inputs to be amplified by the longer portion of e-beam in the seeded simulations. The current profile of the short e-beam is a $T = 2\pi\tau_c = 0.67$ fs duration flattop with 6 kA peak current and 3 MeV energy spread ($\rho = 2.7 \times 10^{-3}$, $\tau_c = 0.11$ fs). This corresponds to a compressed portion of the long e-beam, which is a 30 fs flattop with 1 kA peak current and 0.5 MeV energy spread ($\rho = 1.5 \times 10^{-3}$). The beta function of both beams is 12 m, and a 0.35 μm normalized transverse emittance is assumed, though at these example SXR wavelengths the FEL performance is relatively insensitive to the emittance. We note that the short SASE pulse is fairly insensitive to the precise shape of the ultrashort beam current profile due to the strong slippage effects.

The temporal and spectral profiles of the short pulse and of the amplified seed pulse are shown in Fig. 3. Shot noise is included in all simulations. Early in the linear regime, the short pulse exhibits a well-known "shark fin" temporal profile [Fig. 3(a)] from the flattop short e-beam [28,29]. Because of slippage, the pulse evolves into a 2 fs long, 6 GW (7 μJ) Gaussian-like pulse near saturation [Fig. 3(c)]. It has small temporal modulations from the 1 m drifts between 3.4 m long undulator modules. By saturation, the radiation mode is fully formed and has near full transverse coherence [Fig. 3(d) inset] [30,31]. At $z = 40$ m the short pulse is frequency filtered through the mono, which stretches it to a Gaussian temporal pulse with 9 fs

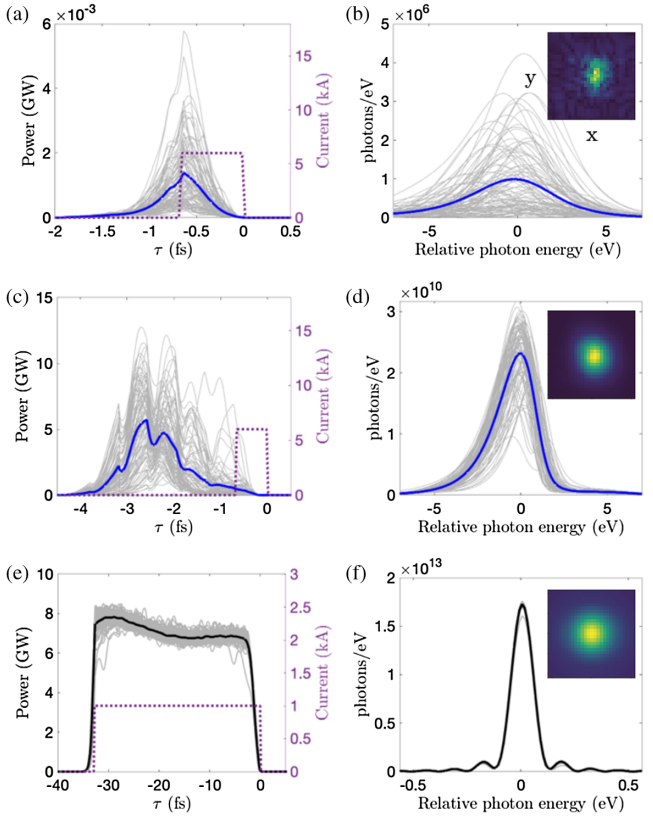

FIG. 3. Radiation temporal profiles and spectra of the short SASE pulse (blue) at $z = 10$ m (a),(b) and $z = 40$ m (c),(d), and of the amplified seed (black) at the $z = 70$ m saturation point (e), (f) for 100 GINGER simulations of lasing at 620 eV. The flattop electron beam current profiles are shown with dashed lines, with the head to the left. The inset shows the single shot transverse radiation mode intensity over a 100 μm window from GENESIS.

FWHM duration and 1 MW average peak power (0.01 μJ pulse energy). It is then amplified by the 30 fs long e-beam, for which the effective shot noise power is about 0.5 kW. By saturation in the seeded stage (which is untapered but detuned by $\Delta\omega/\omega_0 = 0.25\%$ to increase the output power), the 7 GW (225 μJ) radiation pulse displays the flattop temporal profile of the long e-beam [Fig. 3(e)] with $<4\%$ rms instantaneous intensity fluctuations, and has an associated stable, highly coherent narrow-band spectrum with 120 meV FWHM bandwidth [Fig. 3(f)]. Start-to-end simulations with a full nonideal beam tracked with the codes IMPACT [32], ELEGANT [33], and GENESIS [26] show similar results (see Supplemental Material [19]).

The evolution of the pulse energy and of the fluctuations in each stage is shown in Fig. 4. The short pulse shows strong fluctuations in the linear regime that drastically reduce around $z = 30$ m where it starts to saturate [Fig. 4(a)]. Deeper in saturation, the short pulse is most stable ($\sigma_\mathcal{E} \approx 20\%$), but too far into saturation the spectrum can become multispiked. In the seeded FEL, the statistical intensity fluctuations are fixed by the input seed statistics through the linear regime, and then drop significantly to

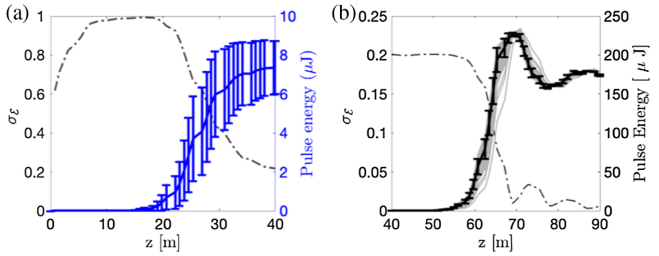

FIG. 4. Statistical fluctuations and gain curve for short SASE pulse (a) and seeded pulse (b) simulated for LCLS-II with GINGER. After the seed is monochromatized at the $z = 40$ m point, it has $\sigma_\mathcal{E} = 20\%$ fluctuations and 1 MW power. After amplification to 7 GW, the fluctuations drop below 4%, reaching 1% at saturation at $z = 70$ m.

$\sigma_\mathcal{E} \approx 1\%$ as the system saturates at $z = 70$ m. This performance stability resembles a conventional optical laser [34].

An important question is how sensitive the FEL output is to the length of the ultrashort e-beam. As shown in Fig. 5(a), for a fixed 6 kA current, we find that a change in the e-beam length over the range $2\pi\tau_c \leq T \leq 4\pi\tau_c$ has little impact on the relative fluctuations through the narrow-band mono, similar to Ref. [24]. The short beam $\pi\tau_c$ does not reach saturation at the mono position and thus has larger fluctuations. Beams longer than $4\pi\tau_c$ begin to develop multiple frequency spikes which also increases fluctuations within the narrow line width.

Another issue is the robustness of the seeded FEL to variations in seed power. In practice, if the short e-beam duration or current fluctuates (e.g., from compression jitter), it changes the spectral brightness (photons/ eV) at the mono, and therefore the pulse power in the seed. For example, in the LCLS-II case, the filtered seed power for the pulse from the $2\pi\tau_c$ beam is 1 MW, while for the $4\pi\tau_c$ beam it is 4.5 MW. This issue is explored in Fig. 5(b), where we show results from a scan over the seed pulse power from 0.1–10 MW ($0.002 - 0.2$ μJ) in steps of

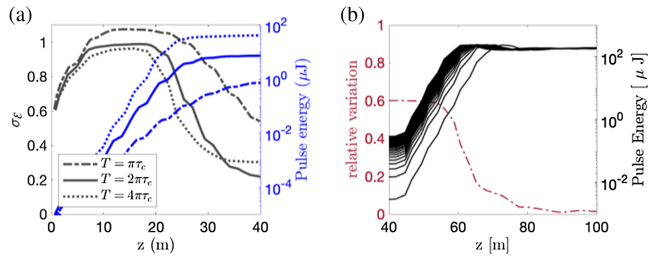

FIG. 5. (a) Total average pulse energy in the SASE section and relative fluctuations through a narrow-band filter for different durations T of the short e-beam. Results are from 500 GINGER simulations for each T. (b) FEL pulse energy in the seeded section for different input seed pulse energies. The rms variation in FEL pulse energy across these values is also shown. It drops to 1% near the $z = 90$ m point, indicating little sensitivity to the input seed power level.

0.4 MW. During exponential gain the seeded FEL power naturally depends on the input seed power. Shortly after saturation, however, it is virtually independent of the seed power, as indicated by the $< 4\%$ rms variation in energy beyond $z = 80$ m over the full range of input powers. The spectra are all virtually identical. This indicates that, when seeded with the single spike high power pulse from the short beam, the saturated seeded FEL is highly insensitive to fluctuations in seed power, as expected [35].

The broad coherent bandwidth incident on the mono allows the possibility to tailor the coherent properties of the FEL, similar to techniques pioneered in external seeding (e.g., Ref. [36]). With customized monochromators, one could envision self-seeding with tunable coherent bandwidths or multiple well-defined and phase-stable frequencies. For example, at SXR wavelengths a dual-color grating (enabled by two superimposed or alternating line densities) could select two colors within the FEL bandwidth, similar to two-color seeding explored at hard x rays [37]. Shown in Fig. 6 are the results of simulations where the 620 eV short pulse spectrum in Fig. 3(d) is filtered by two $\sigma_m = 85$ meV Gaussian apertures separated by 1 eV. The total 0.5 MW input power is split between the colors, which produce a beat modulation on the temporal profile in the seeded section. This modulation persists over multiple shots, indicating high phase stability between the two colors. Similar to a single color, the total energy fluctuations in the amplified two-colors drop to $\sigma_\mathcal{E} \leq 5\%$ at saturation. Further into saturation, additional sideband frequencies also appear at 1 eV intervals out to the edges of the FEL bandwidth, but do not strongly impact the total statistics. Though not observed in this example, we note that in regions where the seeding is weak, such as near the e-beam head or tail or within the temporal beat, SASE can develop and produce a small spectral pedestal, especially near saturation.

In summary, we find that the proposed enhanced self-seeding approach may be used to overcome fundamental limitations in conventional self-seeding. By spectrally filtering pulses from an ultrashort e-beam at saturation, this enables highly stable, fully coherent, and customizable x rays from modern FELs.

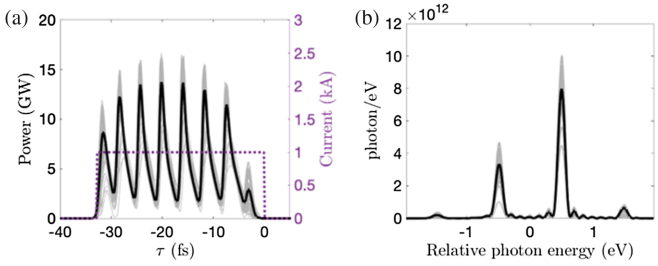

FIG. 6. Temporal (a) and spectral (b) amplified two-color seed pulse profiles at saturation ($z = 80$ m). Results are from 100 GINGER LCLS-II simulations using two colors filtered from the short pulse spectrum centered at 620 eV.

The authors acknowledge helpful conversations with R. Schoenlein, and assistance from W. M. Fawley and G. Marcus on simulations and J. Hastings, S. Serkez, and G. Wilcox on potential two-color grating designs. This work was supported by U.S. Department of Energy Contract No. DE-AC02-76SF00515 and Award No. 2017-SLAC-100382.

*ehemsing@slac.stanford.edu
†aliaksei@slac.stanford.edu
‡zzhang@slac.stanford.edu

[1] E. L. Saldin, E. A. Schneidmiller, and M. V. Yurkov, Opt. Commun. **148**, 383 (1998).
[2] J. Feldhaus, E. Saldin, J. Schneider, E. Schneidmiller, and M. Yurkov, Nucl. Instrum. Methods Phys. Res., Sect. A **393**, 162 (1997).
[3] G. Geloni, V. Kocharyan, and E. Saldin, J. Mod. Opt. **58**, 1391 (2011).
[4] D. Ratner, R. Abela, J. Amann, C. Behrens, D. Bohler, G. Bouchard, C. Bostedt, M. Boyes, K. Chow, D. Cocco *et al.*, Phys. Rev. Lett. **114**, 054801 (2015).
[5] J. Amann, W. Berg, V. Blank, F.-J. Decker, Y. Ding, P. Emma, Y. Feng, J. Frisch, D. Fritz, J. Hastings *et al.*, Nat. Photonics **6**, 693 (2012).
[6] R. Bonifacio, C. Pellegrini, and L. Narducci, Opt. Commun. **50**, 373 (1984).
[7] Z. Zhang, G. Marcus, E. Hemsing, W. M. Fawley, Z. Huang, and A. Lutman, Phys. Rev. Accel. Beams **23**, 010704 (2020).
[8] C. Emma, K. Fang, J. Wu, and C. Pellegrini, Phys. Rev. Accel. Beams **19**, 020705 (2016).
[9] E. Hemsing, A. Halavanau, and Z. Zhang, Phys. Rev. Accel. Beams **23**, 010701 (2020).
[10] R. J. Glauber, Phys. Rev. **130**, 2529 (1963).
[11] O. Y. Gorobtsov, G. Mercurio, F. Capotondi, P. Skopintsev, S. Lazarev, I. A. Zaluzhnyy, M. B. Danailov, M. Dell'Angela, M. Manfredda, E. Pedersoli, L. Giannessi, M. Kiskinova, K. C. Prince, W. Wurth, and I. A. Vartanyants, Nat. Commun. **9**, 4498 (2018).
[12] J. Rosenzweig *et al.*, Nucl. Instrum. Methods Phys. Res., Sect. A **593**, 39 (2008).
[13] S. Huang, Y. Ding, Y. Feng, E. Hemsing, Z. Huang, J. Krzywinski, A. A. Lutman, A. Marinelli, T. J. Maxwell, and D. Zhu, Phys. Rev. Lett. **119**, 154801 (2017).
[14] J. Duris *et al.*, Nat. Photonics **14**, 30 (2020).
[15] J. P. MacArthur, J. Duris, Z. Zhang, A. Lutman, A. Zholents, X. Xu, Z. Huang, and A. Marinelli, Phys. Rev. Lett. **123**, 214801 (2019).
[16] Z. Zhang, J. Duris, J. P. MacArthur, Z. Huang, and A. Marinelli, Phys. Rev. Accel. Beams **22**, 050701 (2019).
[17] C. Emma, Y. Feng, D. C. Nguyen, A. Ratti, and C. Pellegrini, Phys. Rev. Accel. Beams **20**, 030701 (2017).
[18] A. Halavanau, F.-J. Decker, C. Emma, J. Sheppard, and C. Pellegrini, J. Synchrotron Radiat. **26**, 635 (2019).
[19] See Supplemental Material at http://link.aps.org/supplemental/10.1103/PhysRevLett.125.044801 for example start-to-end simulations that use two lasers in the laser heater to shape the electron beam current profile.
[20] A. Marinelli, R. Coffee, S. Vetter, P. Hering, G. N. West, S. Gilevich, A. A. Lutman, S. Li, T. Maxwell, J. Galayda, A. Fry, and Z. Huang, Phys. Rev. Lett. **116**, 254801 (2016).
[21] A. A. Lutman, T. J. Maxwell, J. P. MacArthur, M. W. Guetg, N. Berrah, R. N. Coffee, Y. Ding, Z. Huang, A. Marinelli, S. Moeller, and J. C. U. Zemella, Nat. Photonics **10**, 745 (2016).
[22] Z. Huang and G. Stupakov, Phys. Rev. ST Accel. Beams **8**, 040702 (2005).
[23] C. Emma, A. Lutman, M. W. Guetg, J. Krzywinski, A. Marinelli, J. Wu, and C. Pellegrini, Appl. Phys. Lett. **110**, 154101 (2017).
[24] E. Saldin, E. Schneidmiller, and M. Yurkov, in *Free Electron Lasers 2002*, edited by K.-J. Kim, S. Milton, and E. Gluskin (Elsevier, Amsterdam, 2003), pp. 101–105.
[25] V. Ayvazyan *et al.*, Nucl. Instrum. Methods Phys. Res., Sect. A **507**, 368 (2003).
[26] S. Reiche, Nucl. Instrum. Methods Phys. Res., Sect. A **429**, 243 (1999).
[27] W. M. Fawley, LBNL Technical Report No. LBNL-49625, 2002.
[28] R. Bonifacio, C. Maroli, and N. Piovella, Opt. Commun. **68**, 369 (1988).
[29] S. Y. Cai, J. Cao, and A. Bhattacharjee, Phys. Rev. A **42**, 4120 (1990).
[30] S. Krinsky and L. H. Yu, Phys. Rev. A **35**, 3406 (1987).
[31] E. Saldin, E. Schneidmiller, and M. Yurkov, Opt. Commun. **186**, 185 (2000).
[32] J. Qiang, R. D. Ryne, S. Habib, and V. Decyk, J. Comput. Phys. **163**, 434 (2000).
[33] M. Borland, in *6th International Computational Accelerator Physics Conference (ICAP 2000)* (AIP Publishing, Darmstadt, 2000).
[34] J. Goodman, *Statistical Optics, Wiley Series in Pure and Applied Optics* (Wiley, New York, 2000).
[35] K.-J. Kim, Phys. Rev. Lett. **57**, 1871 (1986).
[36] D. Gauthier, P. R. Ribič, G. De Ninno, E. Allaria, P. Cinquegrana, M. B. Danailov, A. Demidovich, E. Ferrari, and L. Giannessi, Phys. Rev. Lett. **116**, 024801 (2016).
[37] A. A. Lutman, F.-J. Decker, J. Arthur, M. Chollet, Y. Feng, J. Hastings, Z. Huang, H. Lemke, H.-D. Nuhn, A. Marinelli *et al.*, Phys. Rev. Lett. **113**, 254801 (2014).